CHINESE JOURNAL OF MECHANICAL ENGINEERING
Vol. 28, No. 3, 2015

DOI: 10.3901/CJME.2015.0121.017, available online at www.springerlink.com; www.cjmenet.com; www.cjme.com.cn

Effects of Joint Controller on Analytical Modal Analysis of Rotational Flexible Manipulator

CHU Ming*, ZHANG Yanheng, CHEN Gang , and SUN Hanxu

Automation School, Beijing University of Posts and Telecommunications, Beijing 100876, China

Received September 22, 2014; revised January 16, 2015; accepted January 21, 2015

Abstract: Modal analysis is a fundamental and important task for modeling and control of the flexible manipulator. However, almost all of the traditional modal analysis methods view the flexible manipulator as a pure mechanical structure and neglect feedback action of joint controller. In order to study the effects of joint controller on the modal analysis of rotational flexible manipulator, a closed-loop analytical modal analysis method is proposed. Firstly, two exact boundary constraints, namely servo feedback constraint and bending moment constraint, are derived to solve the vibration partial differential equation. It is found that the stiffness and damping gains of joint controller are both included in the boundary conditions, which lead to an unconventional secular term. Secondly, analytical algorithm based on Ritz approach is developed by using Laplace transform and complex modal approach to obtain the natural frequencies and mode shapes. And then, the numerical simulations are performed and the computational results show that joint controller has pronounced influence on the modal parameters: joint controller stiffness reduces the natural frequency, while joint controller damping makes the shape phase non-zero. Furthermore, the validity of the presented conclusion is confirmed through experimental studies. These findings are expected to improve the performance of dynamics simulation systems and model-based controllers.

Keywords: flexible manipulator, analytical modal analysis, boundary constraints, joint controller

1 Introduction

Ever increasing demands for high-speed performance and low-energy consumption of robot system require light-mass designs in the aerospace field. As a result, the manipulators equipped with deployable joints and lightweight links have gained widespread application. The control performance of such flexible mechanisms is strongly dependent on a more accurate dynamics model. In recent years, many studies on the dynamics and control problem of flexible manipulator have been implemented[1–4]. To model a flexible manipulator, modal analysis in conjunction with the classical multibody dynamics theory is the most common approach[5–6]. In other words, the flexible modes have to be defined or evaluated in advance of the multibody dynamics analysis. Therefore, continuing researches on the modal characteristics of such flexible structure have been conducted over the past several decades to predict the modal parameters such as natural frequencies, mode shapes, and damping ratios[7–8].

Mainly based on the consideration of mechanical component parameters, some efforts have been made to discover the effects of a hub-joint and an attached-payload on a flexible link. The frequencies and mode shapes of the flexible manipulator are parameterized in two ratios of link to joint: one is the moment of inertia and the other is the bending stiffness[9]. The study on the changes in link natural frequencies due to the changes in joint stiffness is performed to analyze the relationship between joint and link[10–11]. In addition, MEHREZ, et al[12], examined the vibrations of a flexible link affected by joint inertia. On the other hand, the vibration of a flexible manipulator carrying a payload is very different from the one without attached-payload. For this reason, more attention has been paid to discussing the influences of a tip payload[13–14], a time-varying end mass[15] and an attached mass in an arbitrary settling position[16] on a flexible link, and some explicit expression of the characteristic equation and parametric study are provided in relevant literature. However, almost all of the above-mentioned studies take the manipulator for a purely mechanical structure without considering the feedback action of joint controller.

In the strict sense, the dynamics response of an active mechanism is decided by the interaction between controller and mechanical components[17]. When performing modal analysis of active flexible systems, a multidisciplinary challenge is to discuss the effects of controllers. As far as control of flexible manipulator is concerned, general

* Corresponding author. E-mail: chuming_bupt@bupt.edu.cn
Supported by National Natural Science Foundation of China(Grant No. 51305039), Specialized Research Fund for the Doctoral Program of Higher Education, China(Grant No. 20110005120004), Fundamental Research Funds for the Central Universities, China(Grant No. 2014PTB-00-01), and National Basic Research Program of China(973 Program, Grant No. 2013CB733000)

actuators can be partitioned into two types, namely, distributed actuator(e.g., piezoceramic, which is bonded on the surface of link) and centralized actuator (e.g., motor, which is arranged in the hub-joint). It has been shown that piezoceramic, as a smart material, is often utilized to add active stiffening and damping to improve the behavior of vibration control[18]. Modal analysis of an active flexible manipulator involving the action of collocated piezoelectric actuators has received expected attention in recent years, but still few results can be addressed. For example, the influences of active stiffening and damping introduced by collocated piezoelectric actuators on a composite beam are studied to implement vibration control[19]. The exact mode shapes and natural frequencies associated with the flexural motion of a flexible beam are computed for various piezoceramic distributed actuator arrangements[20–21]. As is well known, the finite element method (FEM) is one of the best tools for performing modal analysis of flexible structures due to its multidisciplinary modeling capabilities. For a comprehensive survey of the finite element modeling of active structures, interested readers can consult the paper written by BENJEDDOU[22]. The latest research reveals how a finite element model of an active mechanism can be modified by equivalent mechanical properties that represent the controller, and how a controller influences mechanical system properties[23]. Nevertheless, one major bottleneck in utilizing finite element models is the large number of state variables which in turn, contributed to an ill-condition control problem. Generally speaking, the analytical approach based on vibration partial differential equation (VPDE) is a widespread and efficient method in the analysis of flexible multibody systems. To the best of our knowledge, in the openly published literature there is no research on analytical modal analysis of active flexible manipulator involving the action of centralized actuator, which aims to perform rotational moments.

The objective of this paper is to improve the accuracy of closed-loop modal analysis of rotational flexible mechanisms driven by joint controller. We investigated the analytical modal analysis of an active flexible manipulator with deployable joint. The joint controller is limited to be of type proportional derivative(PD), which is the most common type of joint controller in use today[24–25]. The derived results are compared to the modal parameters of a conventional clamped link so as to highlight the effects of joint controller.

2 Vibration Model of Rotational Flexible Manipulator

Fig. 1 shows a schematic illustration of a rotational flexible manipulator.

The Euler-Bernoulli beam is selected as the dynamics model for the flexible link due to its dimension. $\boldsymbol{M}$ denotes the mass matrix, and $\boldsymbol{K}$ denotes the stiffness matrix. For an evident influence of joint controller in the latter analysis here, the damping of mechanism and material are both purposefully ignored and then $u(x, t)$ can be assumed to satisfy the following VPDE:

$$\begin{cases} \boldsymbol{M}\ddot{u} + \boldsymbol{K}u = 0, \\ \boldsymbol{M} = \rho A, \\ \boldsymbol{K} = EI\partial^4 / \partial x^4. \end{cases} \tag{1}$$

Where ρ denotes the mass density, A cross-sectional area, E Young's modulus, and I the geometrical moment of inertia.

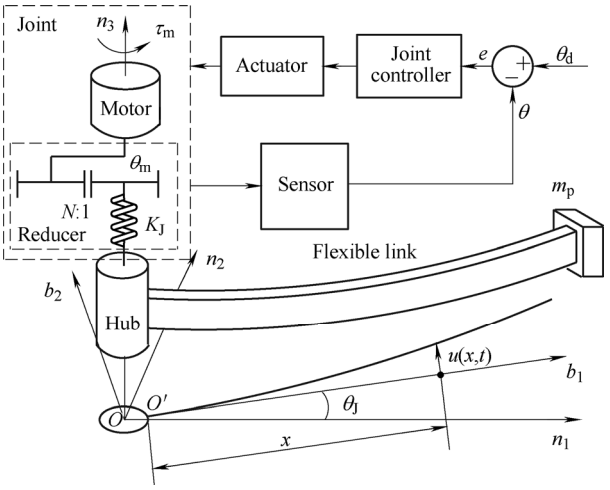

Fig. 1. Configuration of rotational flexible manipulator with joint controller

$O\boldsymbol{n}_1\boldsymbol{n}_2\boldsymbol{n}_3$—Global coordinate system;
$O\boldsymbol{b}_1\boldsymbol{b}_2\boldsymbol{n}_3$—Locally siamesed coordinate system added to the flexible link. The orientation of $\boldsymbol{b}_1$-axis is always tangential with deformed link at the point O', where link attaching to the hub. Neglecting gravity, only transverse vibration is considered;
θ—Joint shaft angular position about $\boldsymbol{n}_3$-axis;
θ_d—Reference variable;
e—Tracking error between θ and θ_d;
θ_J—Hub position;
θ_m—Motor shaft position;
N—Reduction ratio;
K_J—Joint's torsion stiffness coefficient;
τ_m—Controller output torque;
$u(x, t)$—Vibration displacement as a function of the link's length coordinate x and time t;
m_p—Tip payload.

According to Ritz approach, $u(x, t)$ and the ith order vibration displacement $u_i(x, t)$ are expressed as

$$\begin{cases} u(x,t) = \sum_{i=1}^{\infty} u_i(x,t), \\ u_i(x,t) = \varphi_i(x)\sin(\omega_i t). \end{cases} \tag{2}$$

Where $\varphi_i(x)$ is the ith order mode shape and ω_i is the ith angular frequency. Further more, the VPDE can be solved by the following function:

$$\varphi_i(x) = A_i \sin(k_i x) + B_i \cos(k_i x) + C_i \sinh(k_i x) + D_i \cosh(k_i x), \tag{3}$$

where k_i=sqrt(ω_i/γ) and γ=sqrt($EI/\rho A$). These four constants, A_i, B_i, C_i and D_i, have to be evaluated using appropriate boundary conditions. The kinematical boundary conditions result from pure geometrical compatibility and describe geometrical constraints, while the dynamical boundary conditions express information on the internal forces or moments at the considered boundary. Quite often the appropriateness of these boundary conditions is a point of discussion[26], where the definition of constraint would lead to strictly different dynamics responses. The kinematical and dynamical boundary conditions supplement each other and their satisfaction ensures that the solution of the VPDE is unique. Thus, if the actions of joint controller are known, they can be expressed in the boundary equations.

3 Analytical Modal Analysis with the Effects of Joint Controller

3.1 Controller feedback constraint and boundary conditions

For a rotational manipulator, common control design is to perform trajectory planning, trajectory tracking and set-point regulation, etc. In most cases, an expected continuous trajectory can always be divided into a limited number of discrete points and every corresponding position is as the reference input to the controller. Thus, an important task for the controller is to track all the input variables during the servo process. Let us first investigate the dynamic adjustment in controller based on state feedback. To implement a large-scale motion, the deployable joint reaches each discrete reference position with the occurrence of link vibration due to its flexibility. At this time, the joint position tracking error e emerges as a result of the bending moment at link root, and therefore joint controller has to output a torque τ_m to rectify the deviation and locate the link root. It needs to be pointed out that τ_m is produced by e and $\dot{e}$ in PD type position controller, as shown in Fig. 2. For position feedback controller, the proportional gain K_p affects the stiffness, whereas the derivative gain K_d affects the damping of the closed-loop system. Hence, the flexible link is really a cantilever-like model driven by the control torque τ_m at root rather than a static clamped beam. In this section, we revealed how the servo stiffness and damping from controller are introduced into the constraint equation of flexible link boundary conditions.

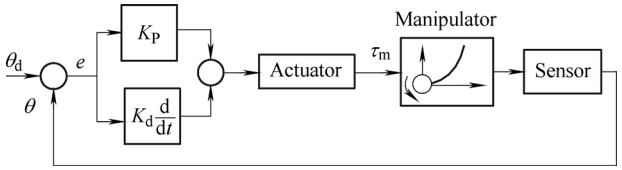

Fig. 2. Block diagram for rotational flexible manipulator with joint controller

Firstly, the joint position tracking error e can be expressed as

$$\begin{cases} e = \theta_d - \theta, \\ \theta = \theta_J + \xi + u'(0,t). \end{cases} \tag{4}$$

Where ξ is the torsional spring deformation in reducer and $u'(0,t)$ represents the additional angle at the link root induced by transverse vibration. At each discrete relative equilibrium position, there exists the equation θ_d=θ_J. Hence, the resulting equation by Eq. (4) is given by

$$\begin{cases} e = -\xi - u'(0,t), \\ \xi = \theta_m / N - \theta_J. \end{cases} \tag{5}$$

Considering the internal moment, the balance formula can be obtained as

$$N(\tau_m - J_m\ddot{\theta}_m) = K_J\xi, \tag{6}$$

where J_m is motor shaft inertia. For a feedback PD-type controller shown in Fig. 2, the controller output torque τ_m can be written as

$$\tau_m = K_p e + K_d\dot{e}. \tag{7}$$

It is implied that the controller gains K_p and K_d are both positive. In what follows, we sought the kinematical and dynamical boundary conditions of the flexible link.

For x=0 (i.e., at the root of the link):

$$u(0,t) = 0, \tag{8}$$

$$J_J[\ddot{u}'(0,t) + \ddot{\boldsymbol{\xi}}] = K_J\boldsymbol{\xi} + EIu''(0,t), \tag{9}$$

where J_J is hub inertia.

For x=L (i.e., at the end of the link):

$$EIu''(L,t) = 0, \tag{10}$$

$$EIu'''(L,t) = m_p\ddot{u}(L,t), \tag{11}$$

where L is link length.

In an actual system, since both J_m and J_J are relatively infinite-small parameters, the terms including these two variables are all neglected. Combining Eqs. (5)–(9) yields a new equation as

$$K_pu'(0,t) + K_d\dot{u}'(0,t) = \left(\frac{K_p}{K_J} + \frac{1}{N}\right)EIu''(0,t) + \frac{K_d}{K_J}EI\dot{u}''(0,t). \tag{12}$$

Thus, Eqs. (8), (10)–(12) describe the exact boundary

conditions, which are specially used to solve the above-mentioned four constants A_i, B_i, C_i and D_i.

3.2 Modal analysis in frequency domain

As for all the terms including $\dot{u}'(0,t)$ and $\dot{u}''(0,t)$ in Eq. (12), it is implied that a secular term, i.e., $\cos(\omega_i t)$, which is an obstacle for solving the VPDE in time domain, would inevitably appear in the frequency equation. That is due to the resulting equations by Eq. (2):

$$\begin{cases}\dot{u}'(0,t)=\omega_i\varphi_i'(0)\cos(\omega_i t),\\ \dot{u}''(0,t)=\omega_i\varphi_i''(0)\cos(\omega_i t).\end{cases}$$

Therefore, here the Laplace transforming method is employed in order to convert Eq. (2) from time domain to frequency domain, and the Laplace description of Eq. (2) is given as

$$u_i(x,s)=\varphi_i(x)\frac{\omega_i}{s^2+\omega_i^2}, \tag{13}$$

where s is the Laplacian. Substitute Eqs. (3) and (13) into Eq. (1), then the following formula can be obtained:

$$k_i^4=-\frac{\rho A}{EI}s^2=-\frac{1}{\gamma^2}s^2. \tag{14}$$

Setting a new variable $\lambda_i=k_iL$, and combining Eqs. (3), (8), (10)–(13) yields the corresponding consistent linear equations with respect to the four constants A_i, B_i, C_i and D_i as

$$\begin{cases}B_i=-D_i,\\ \boldsymbol{F}\begin{pmatrix}A_i\\C_i\\D_i\end{pmatrix}=\begin{pmatrix}f_{11}&f_{12}&f_{13}\\f_{21}&f_{22}&f_{23}\\f_{31}&f_{32}&f_{33}\end{pmatrix}\begin{pmatrix}A_i\\C_i\\D_i\end{pmatrix}=0.\end{cases} \tag{15}$$

Where $f_{11}=-\sin\lambda_i, f_{12}=-\sinh\lambda_i, f_{13}=\cos\lambda_i+\cosh\lambda_i,$

$f_{21}=-EI\lambda_i^3\cos\lambda_i/L^3-m_{\mathrm{p}}s^2\sin\lambda_i,$

$f_{22}=EI\lambda_i^3\cosh\lambda_i/L^3-m_{\mathrm{p}}s^2\sinh\lambda_i,$

$f_{23}=EI\lambda_i^3(\sinh\lambda_i-\sin\lambda_i)/L^3-m_{\mathrm{p}}s^2(\cosh\lambda_i-\cos\lambda_i),$

$f_{31}=(K_{\mathrm{p}}+K_{\mathrm{d}}s)\lambda_i/L, f_{32}=f_{31},$

$f_{33}=-2EI\,[(K_{\mathrm{p}}+K_{\mathrm{d}}s)/K_{\mathrm{J}}+1/N]\lambda_i^2/L^2.$

The complex expression of Laplacian s in Eq. (15) can be derived from Eq. (14), that is

$$s=\pm\mathrm{j}\gamma k_i^2=\pm\mathrm{j}\gamma\lambda_i^2/L^2, \tag{16}$$

where j is the imaginary unit. By selecting $s=-\mathrm{j}\gamma\lambda_i^2/L^2$, the frequency equation can be given as

$$\det\boldsymbol{F}=0. \tag{17}$$

Solving Eq. (17) with respect to λ_i gives λ_i as a complex number owing to the introduction of j. Suppose that the ith-order complex frequency eigenvalue λ_i can be written as

$$\begin{cases}\lambda_i=-\sigma_i+\mathrm{j}\nu_i,\\ \overline{\lambda}_i=-\sigma_i-\mathrm{j}\nu_i.\end{cases} \tag{18}$$

Where the imaginary part represents the frequency of vibration, and the real part represents the constant in the exponent of the vibration amplitude envelope. If the real part is positive, the vibration is growing, which means that the system is unstable. This can occur as a result of setting inappropriate gains in the joint controller design, for example, a negative proportional gain or derivative gain. Since the real part of λ_i, which leads to vibration attenuation, is really introduced by the controller term $K_{\mathrm{d}}\dot{e}$, it is certain that the damping is completely produced by the joint controller. For a general expression, the ith-order damped angular frequency ω_i and equivalent damping ratio ζ_i are given by

$$\begin{cases}\omega_i=\gamma\nu_i^2/L^2,\\ \zeta_i=\mathrm{sqrt}[1-(\omega_i/\omega_{0i})^2],\end{cases} \tag{19}$$

where ω_{0i} is the undamped natural frequency. It is worth mentioning that the equivalent damping ratio ζ_i in Eq. (19) is different from the conventional damping ratio owing to the different constraint types and boundary conditions. ζ_i is only used to reflect the effect of joint controller on modal frequency, and the damped frequency ω_i has consequently lowered. After solving the frequency eigenvalue, substituting λ_i into Eq. (3) yields the mode shape function.

For $m_{\mathrm{p}}=0$:

$$\varphi_i(x)=D_i\{(a_i-b_i)\sin(\lambda_i x/L)+b_i\sinh(\lambda_i x/L)+\left[\cosh(\lambda_i x/L)-\cos(\lambda_i x/L)\right]\}, \tag{20}$$

where $a_i=2\lambda_i EI\left[\dfrac{1}{K_{\mathrm{J}}L}+\dfrac{1}{(K_{\mathrm{p}}-\mathrm{j}K_{\mathrm{d}}\gamma\lambda_i^2/L^2)NL}\right],$

$$b_i=\frac{1+\cosh\lambda_i\cos\lambda_i-\sin\lambda_i\sinh\lambda_i}{\sin\lambda_i\cosh\lambda_i-\cos\lambda_i\sinh\lambda_i}.$$

In addition, the same format for $\overline{\lambda}_i$ can be obtained. From Eq. (20) it is clearly shown that $\varphi_i(x)$ is plural and its general expression can be described as

$$\begin{cases}\varphi_i(x)=\mathrm{Re}[\varphi_i(x)]+\mathrm{j}\,\mathrm{Im}[\varphi_i(x)],\\ \overline{\varphi}_i(x)=\mathrm{Re}[\varphi_i(x)]-\mathrm{j}\,\mathrm{Im}[\varphi_i(x)].\end{cases} \tag{21}$$

Therefore, based on Eqs. (19) and (21), Eq. (2) can be

revised as

$$u_i(x,t) = 2\exp(-\varsigma_i t)\,\text{Re}(\varphi_i)\cos(\omega_i t) - \text{Im}(\bar{\varphi}_i)\sin(\omega_i t)), \tag{22}$$

where the real and imaginary part represents the vibration magnitude and the phase, respectively.

Theorem. When involving the effects of joint controller, the vibration of rotational flexible manipulator is not synchronized.

Proof. Fig. 3 shows the variation curves of output torque τ_m from PD feedback controller by two subgraphs, i.e., subgraph (a) is an illustration of the detached torque by $K_p e$ and $K_d \dot{e}$, subgraph (b) is an illustration of the synthetic torque described by solid green lines. Let $[-e_{max}, +e_{max}]$ denote the mutative interval of e, where e_{max} is the limit position of e. The solid line, which is used to describe the term $K_p e$, represents the servo stiffness of controller; the dotted line, which is used to describe the term $K_d \dot{e}$, represents the servo damping of controller. Subgraph (a) shows the contrary trend between $K_p e$ and $K_d \dot{e}$ with $K_p e$ reaching zero while $K_d \dot{e}$ reversely reaching positive or negative maximum value, or $K_d \dot{e}$ reaching zero while $K_p e$ reversely reaching positive or negative maximum value.

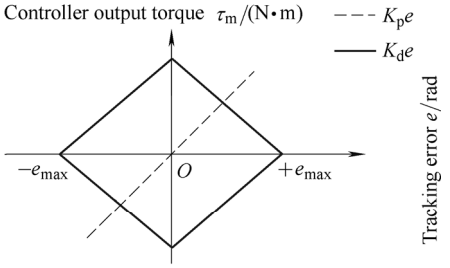

(a) Detached torque

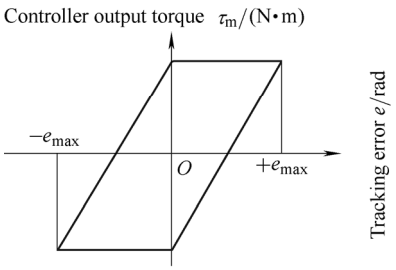

(b) Synthetic torque

Fig. 3. Output torque of joint controller

As is well known, the phase difference of conventional real mode shape is either 0° or 180°, which means that all points on the link reach their equilibrium or maximum position at the same time. However, the effects of joint controller make the phase difference inconsistent. As shown in Eq. (22), the vibration phase with controller gains can be given by

$$\Omega_i = \arctan\frac{\text{Im}(\varphi_i)}{\text{Re}(\varphi_i)}.$$

Since the controller gains K_p and K_d are uncorrelated with each other, the changes of servo stiffness and servo damping are not synchronized. Hence, the internal damping force is not proportional with the local inertial force and elastic force, meaning that not only the mode shape magnitude fluctuates but the phase changes, i.e. the vibration of rotational flexible manipulator is not synchronized.

3.3 Modal analysis in complex domain

Using inverse Laplace tranform method, and combining Eqs. (1), (21) and (22), yields the general VPDE of rotational flexible manipulator as

$$\boldsymbol{M}\ddot{\boldsymbol{u}} + \boldsymbol{C}\dot{\boldsymbol{u}} + \boldsymbol{K}\boldsymbol{u} = 0, \tag{23}$$

where $\boldsymbol{C}$ is the damping matrix induced by joint controller, i.e., it is a non-proportional matrix and can not be decoupled by conventional orthogonal shape approach. Considering the identical equation $\boldsymbol{M}\dot{\boldsymbol{u}} - \boldsymbol{M}\dot{\boldsymbol{u}} = 0$, then Eq. (23) is rewritten as

$$\begin{cases} \boldsymbol{A}\dot{\boldsymbol{y}} + \boldsymbol{B}\boldsymbol{y} = \boldsymbol{0}, \\ \boldsymbol{y}(0) = \boldsymbol{y}_0, \end{cases} \tag{24}$$

where $\boldsymbol{A} = \begin{pmatrix} \boldsymbol{C} & \boldsymbol{M} \\ \boldsymbol{M} & \boldsymbol{0} \end{pmatrix}$, $\boldsymbol{B} = \begin{pmatrix} \boldsymbol{K} & \boldsymbol{0} \\ \boldsymbol{0} & -\boldsymbol{M} \end{pmatrix}$,

$\boldsymbol{y} = \begin{pmatrix} \boldsymbol{u} \\ \dot{\boldsymbol{u}} \end{pmatrix}$, $\boldsymbol{y}_0 = \begin{pmatrix} \boldsymbol{u}_0 \\ \dot{\boldsymbol{u}}_0 \end{pmatrix}$.

Solving Eq. (24) with respect to the vector $\boldsymbol{y}$ gives $\boldsymbol{y}$ as

$$\boldsymbol{y} = \boldsymbol{\Psi}\exp(\lambda t), \tag{25}$$

where λ is the eigenvalue and $\boldsymbol{\Psi}$ is the eigenvector as

$$\boldsymbol{\Psi} = (\boldsymbol{\Psi}_1 \quad \boldsymbol{\Psi}_2 \quad \cdots \quad \boldsymbol{\Psi}_i \quad \cdots),$$

$$\boldsymbol{\Psi}_i = (\varphi_i \quad \lambda_i\varphi_i)^{\mathrm{T}}.$$

Combining Eqs. (24) and (25) yields the eigenvalue equation as

$$\det\left(\boldsymbol{D} - \frac{1}{\lambda}\boldsymbol{I}\right) = 0,$$

where $\boldsymbol{D} = -\boldsymbol{B}^{-1}\boldsymbol{A} = \begin{pmatrix} -\boldsymbol{K}^{-1}\boldsymbol{C} & -\boldsymbol{K}^{-1}\boldsymbol{M} \\ \boldsymbol{I} & \boldsymbol{0} \end{pmatrix}$,

and $\boldsymbol{I}$ is an identity matrix.

Let

$$\boldsymbol{u} = \boldsymbol{\Phi}\exp(\boldsymbol{\Lambda}t),$$

where $\boldsymbol{\Phi} = (\varphi_1 \quad \bar{\varphi}_1 \quad \varphi_2 \quad \bar{\varphi}_2 \quad \cdots \quad \varphi_i \quad \bar{\varphi}_i)$,

$\boldsymbol{\Lambda} = \text{diag}(\lambda_1 \quad \bar{\lambda}_1 \quad \lambda_2 \quad \bar{\lambda}_2 \quad \cdots \quad \lambda_i \quad \bar{\lambda}_i)$.

The coordinate transforming matrix $\boldsymbol{\Psi}$ for decoupling Eq.

(25) is written as

$$\boldsymbol{\Psi} = (\boldsymbol{\Phi} \quad \boldsymbol{\Phi\Lambda})^{\mathrm{T}}. \tag{26}$$

It is implied that $\boldsymbol{\Psi}_i$ is orthogonal about $\boldsymbol{A}$ and $\boldsymbol{B}$, that is

$$\begin{cases} \boldsymbol{\Psi}_i^{\,T} \boldsymbol{A} \boldsymbol{\Psi}_i = a_i, \\ \boldsymbol{\Psi}_i^{\,T} \boldsymbol{B} \boldsymbol{\Psi}_i = \beta_i, \end{cases} \tag{27}$$

where both α_i and β_i are nonzero variables, and therefore the following equation can be derived:

$$\begin{cases} \beta_i = -\lambda_i \alpha_i, \\ \overline{\beta}_i = -\overline{\lambda}_i \overline{\alpha}_i. \end{cases} \tag{28}$$

Thus, let

$$\boldsymbol{y} = \sum_{i=1}^{\infty} \boldsymbol{\Psi}_i q_i, \tag{29}$$

combining Eqs. (24) and (29), the ith decoupled equation can be derived as

$$\alpha_i \dot{q}_i + \beta_i q_i = 0. \tag{30}$$

Solving Eq. (30) with respect to q_i gives q_i as

$$q_i = \frac{\boldsymbol{\Psi}_i^{\,\mathrm{T}} \boldsymbol{A} \boldsymbol{y}_0}{\alpha_i} \exp(\lambda_i t). \tag{31}$$

Finally, combining Eqs. (24), (26), (29) and (31) yields the vibration displacement as

$$\boldsymbol{u}(x,t) = \sum_{i=1}^{\infty} \frac{\varphi_i \varphi_i^{\,\mathrm{T}}}{\alpha_i} \left[\boldsymbol{M}(\dot{\boldsymbol{u}}_0 + \lambda_i \boldsymbol{u}_0) + \boldsymbol{C}\boldsymbol{u}_0 \right] \exp(\lambda_i t). \tag{32}$$

4 Numerical Simulations

To verify the theory derived in the previous paragraphs and illustrate the effects of joint controller with various controller gains, some numerical examples for a single-link rotational flexible manipulator, as shown in Fig. 1, are performed. The link and joint mechanical parameters of the rotational flexible manipulator are listed in Table 1, from which it is clearly seen that the damping of mechanism and material are both purposefully ignored. The intention behind the simulations was to have a simple and verifiable model for verification of the derived theory, as well as to highlight the interaction between controller and mechanical components. All the numerical examples are intended as the illustrative simulations only; therefore, it is deliberately not an exact replication of a real physical product. Because of this, the parameter values used for the manipulator are not of importance in this context.

Table 1. Mechanism parameters of the rotational flexible manipulator

Mass density ρ/(kg • m^{-3})	Cross-sectional area A/m^2	Young's modulus E/GPa
2710	0.030×0.008	71
Link length L/m	**Stiffness coefficient K_J/(Nm • rad^{-1})**	**Reduction ratio N**
1.0	7500	100

Modal analysis of conventional static clamped beam model is given here as a comparison with the rotational flexible manipulator. To perform modal analysis of the manipulator, two different approaches are used:

(1) Unchanged tip-payload with variable controller gains: The tip-payload is a given constant, but the proportional gain and derivative gain are both variables. This approach is mainly used to obtain the modal analysis results from the effects of controller gains.

(2) Variable tip-payload with unchanged controller gains: The proportional gain and derivative gain are both given constants, but the tip-payload is variable. This approach is mainly used to obtain the modal analysis results from the effects of tip-payload.

The objective of the examples with tip-payload is to further illustrate the effects of joint controller. A comparison of the calculated eigenfrequencies derived from clamped link and from rotational flexible manipulator is shown in Table 2. As can be seen, there are evident differences in the

Table 2. Comparison of modal frequency under different tip-payload and joint controller gains

Tip payload m_p/kg	Clamped link		Rotational flexible manipulator with joint controller				
	Frequency f/Hz		Controller gains		Frequency f/Hz	Decline rate /%	Damping ratio ζ_i
			K_p	K_d			
0	1st	6.615	1	0.01	3.033	54.14	0.889
			10	0.01	5.560	15.95	0.542
			50	0.10	6.247	5.56	0.329
	2nd	41.454	1	0.01	31.286	24.53	0.656
			10	0.01	36.406	12.18	0.478
			50	0.10	39.542	4.61	0.300
0.65	1st	2.931	1	0.01	1.472	49.78	0.865
			10	0.01	2.541	13.30	0.498
			50	0.10	2.798	4.52	0.297
	2nd	30.573	1	0.01	22.108	22.69	0.277
			10	0.01	26.715	12.62	0.126
			50	0.10	29.110	4.79	0.048
1.3	1st	2.180	1	0.01	1.107	49.20	0.861
			10	0.01	1.897	13.00	0.493
			50	0.10	2.084	4.42	0.294
	2nd	29.840	1	0.01	21.394	28.30	0.283
			10	0.01	26.022	12.79	0.128
			50	0.10	28.393	4.85	0.048
3.0	1st	1.480	1	0.01	0.758	48.81	0.859
			10	0.01	1.291	12.79	0.489
			50	0.10	1.416	4.34	0.291
	2nd	29.381	1	0.01	20.938	28.74	0.287
			10	0.01	25.586	12.92	0.129
			50	0.10	27.943	4.90	0.049

frequency results from the various controller gains(i.e. different given values combination of K_p and K_d) and from the various tip-payload(i.e. different given values of m_p). All eigenfrequencies derived from clamped link are higher than those from active manipulator with joint controller. For the 1st frequency, under m_p=0, the difference between clamped link and active manipulator is 3.528 Hz (corresponding K_p=1, K_d=0.01), 1.055 Hz(corresp-onding K_p=10, K_d=0.01) and 0.368 Hz(corresponding K_p=50, K_d=0.1), respectively. For the 2nd frequency, under m_p=0, the difference between clamped link and active manipulator is 10.168 Hz (corresponding K_p=1, K_d=0.01), 5.048 Hz (corresponding K_p=10, K_d=0.01) and 1.912 Hz (corresponding K_p=50, K_d=0.1), respectively. From the above variation law, it can be speculated that the frequency of active manipulator would be close to the static clamped link with the continuous increment of K_p and K_d. But for an actual servo system, it is impossible to unrestrictedly enlarge the controller gains, and usually, K_p is defined as a comparatively large variable to ensure the instantaneous action and K_d is defined as a comparatively small variable to regulate the oscillation. Hence, the frequencies of active manipulator would be lower than those of clamped link. The decline-rate in Table 2, which is calculated by $(\omega_{0i}-\omega_i)/\omega_{0i}$, implies the relative degree of frequency change and reflects the action of active control to a mechanism. The damping ratio in Table 2, which is calculated by Eq. (19), reveals the effect of joint controller on modal frequency and is favorable for the stability of oscillation.

The mode shapes of interest(i.e. the first two–order modes) with various controller gains are sketched in Fig. 4, compared with clamped link. In the 1st and 2nd mode shape with joint controller gains(i.e. the red, green and blue solid lines), both the real part deformations have similar, but different, shape with clamped link(i.e. the purple dashed line), whereas the imaginary part deformations have 1st U-shaped and 2nd S-shaped form, respectively. In contrast, the imaginary part of an undamped clamped link is zero, as shown in Fig. 4.

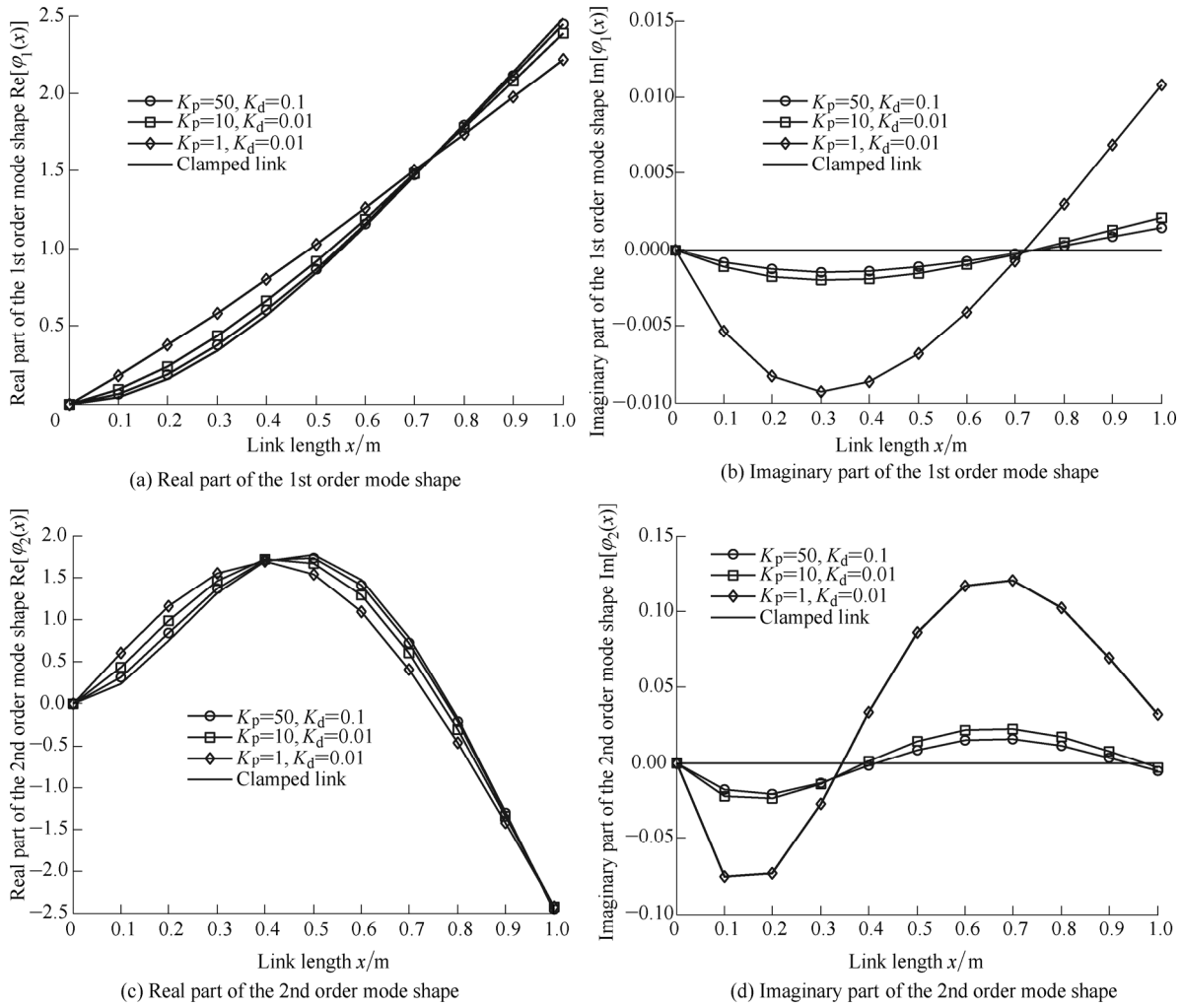

Fig. 4. The 1st and 2nd order mode shapes of rotational flexible manipulator with joint controller, compared with clamped link

In addition, Fig. 5 is an illustration of the 1st and 2nd phases, Ω_1 and Ω_2, derived using formula arctan[Im(φ_i)/Re(φ_i)]. These phase diagrams reflect the existence of non-proportional damping in an active system, which is a further proof of the above proposition. As mentioned in Section 3.2, it is certain that the non-proportional damping is completely produced by the joint controller. Meanwhile, one can see from Figs. 4–5 that as for both the mode shapes

and phases of active manipulator, the lower controller gains, the more obvious differences.

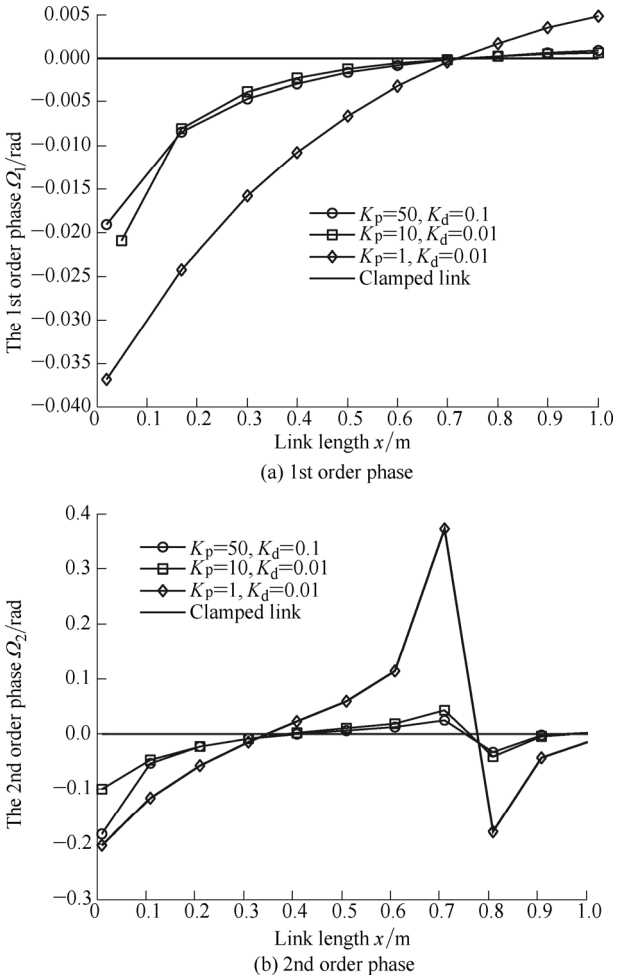

Fig. 5. The 1st and 2nd order phases of rotational flexible manipulator with joint controller, compared with clamped link

From the above comparison, it is confirmed that, as for all the points on the link, there is no instant of reaching equilibrium of maximum position simultaneously, and the vibration displacement ratio is mutative. Thus, the vibration response of active manipulator with joint controller is significantly different from the conventional clamped link. As is well known, modal analysis in conjunction with the classical multibody dynamics theory is the most common approach to modeling a flexible multibody system. Before performing a closed-loop feedback control simulation, more accurate dynamics equations for an active system are necessary to preview the validity of designed control strategy. Although only PD type controller is introduced in this article, the controller gains K_p and K_d can still be equivalent general terms of other types of controller.

To clearly observe the vibration responses of active manipulator with joint controller, several typical time responses in three–dimensional space for the 1st and 2nd deformation about position x and time t are performed. The time simulation ran for 5 s with a time increment of 0.1 s, and the surface plots are given in Fig. 6. One can see that there is an obvious difference in the results of vibration frequency, amplitude, deformation shape and convergence time, etc. due to different combinations of controller gains, namely, the red-surface of K_p=1 and K_d=0.01, the green-surface of K_p=10 and K_d=0.01 and the blue surface of K_p=50 and K_d=0.1.

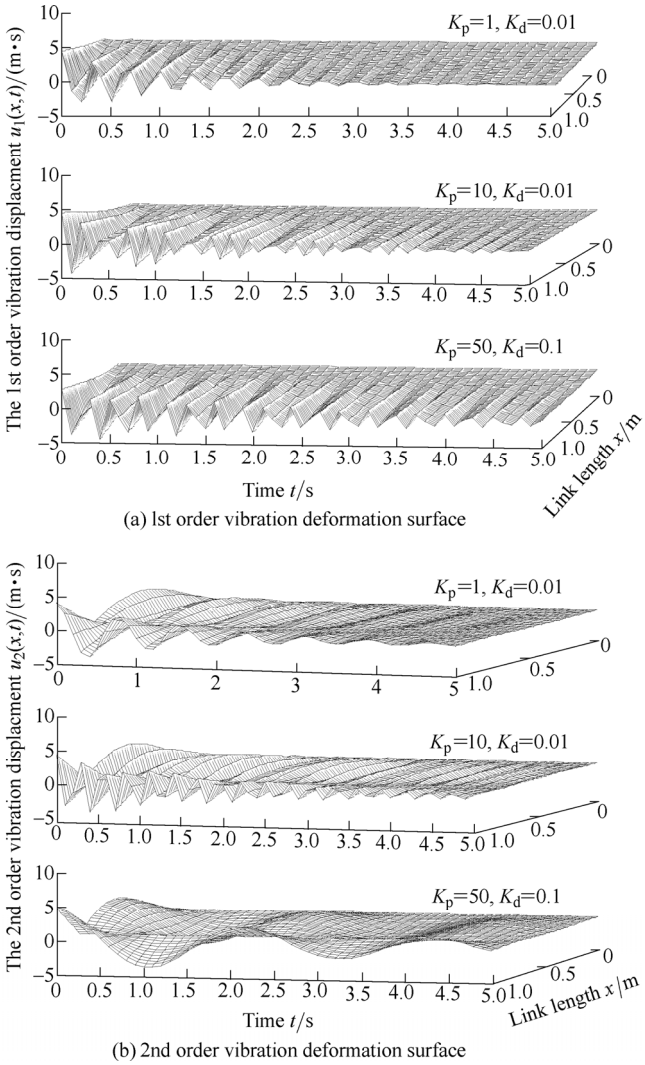

Fig. 6. The 1st and 2nd order vibration deformation surfaces of rotational flexible manipulator with joint controller

5 Experimental Results

In order to evaluate the analytical results obtained in the previous sections and draw a conclusion on the accuracy of the modeling theory adopted, a single rotational flexible manipulator is built. A SGMAH-04AAA41 AC servo motor and a SGDM-04ADA servopack are used as a rotational joint. A PCB 333B32 accelerometer and LMS SCADAS data acquisition are used to collect sets of data and experimentally obtain the natural frequency response of the flexible-link by LMS Test.Lab software package. We purposefully removed the reducer from joint mechanism in order to highlight the effects of joint controller gains, i.e., flexible-link is directly driven by motor. Fig. 7 shows the experimental setup used in this study.

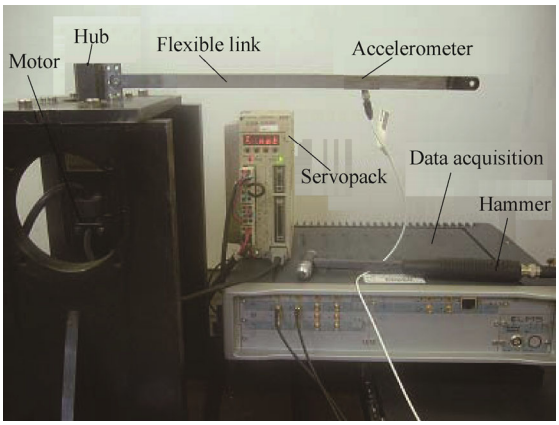

Fig. 7. Experimental setup of rotational flexible manipulator

We first defined different controller gains(i.e. proportional gain K_p and derivative gain K_d) in the servopack, and then obtained different boundary constraints. The modal tests were performed through hammer percussion method. Fig. 8 shows the amplitude-frequency response of rotational flexible manipulator with different joint controller gains and Table 3 gives the first two–order corresponding identified frequency.

Table 3. Comparison of modal frequency of manipulator under different joint controller gains

Modal order	Modal Frequency f / Hz			
	K_p=40, K_d=40	K_p=160, K_d=240	K_p=260, K_d=540	Clamped link
1st	4.60	4.88	5.01	5.48
2nd	22.98	29.81	30.74	32.31

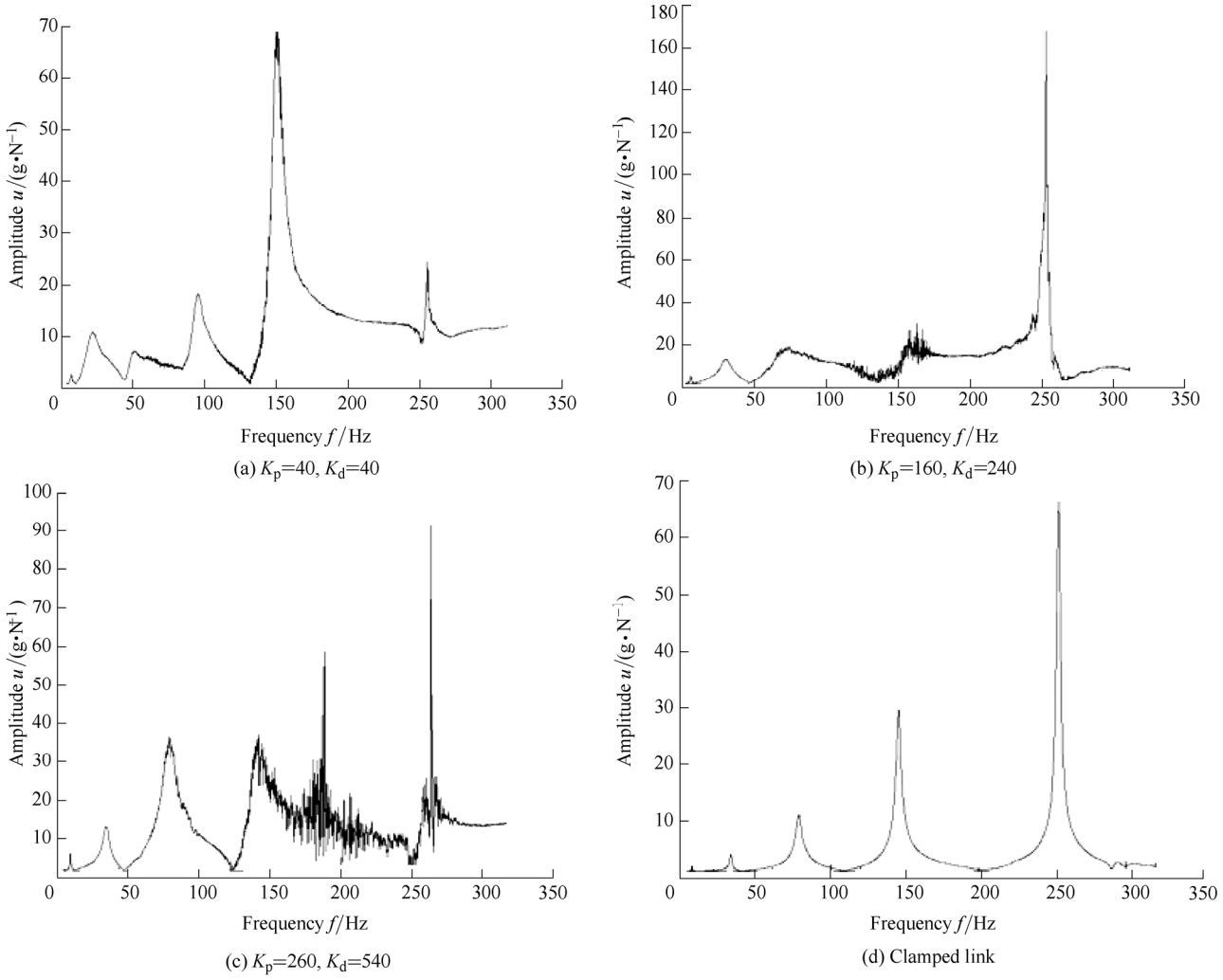

Fig. 8. Modal test for the amplitude-frequency response of rotational flexible manipulator with different joint controller gains

One can see that the experimental results are consistent with the previous theoretical analysis: the frequencies of active manipulator are lower than those of clamped link. In addition, the experimental mode shapes of interest are similar to the numerical simulation results in Fig. 4. It is worth mentioning that only the real part of mode shape can be identified in LMS Test.Lab, and the imaginary part is generally neglected in the commercial software packages. The experimental results demonstrate a significant difference in the accuracy of the modal analysis of an active system and non-active system.

6 Conclusions

(1) According to Ritz approach, the closed-loop vibration partial differential equation of rotational flexible manipulator is derived. Considering the feedback action of joint controller, the kinematical and dynamical boundary

conditions are obtained.

(2) The joint controller stiffness and damping gains are both included in the boundary conditions of VPDE. Joint controller stiffness reduces the manipulator natural frequency, and joint controller damping makes the manipulator shape phase non-zero.

(3) By using Laplace transform and complex modal approach, the analytical algorithm for modal analysis is developed to provide accurate eigenfrequency and mode shape calculations. The simulation and experiment results show a good agreement with theoretical analysis.

References

[1] BIAN Yushu, GAO Zhihui. Impact vibration attenuation for a flexible robotic manipulator through transfer and dissipation of energy[J]. *Shock and Vibration*, 2013, 20(4): 665–680.

[2] BIAN Yushu, GAO Zhihui, YUN Chao. Study on vibration reduction and mobility improvement of the flexible manipulator via redundancy resolution[J]. *Nonlinear Dynamics*, 2011, 65(4): 359–368.

[3] ZHANG Xuping, MILLS J K, CLEGHORN W L. Multi-mode vibration control and position error analysis of parallel manipulator with multiple flexible links[J]. *Transactions of the Canadian Society for Mechanical Engineering*, 2010, 34(2): 197–213.

[4] BIAN Yushu, GAO Zhihui, YUN Chao. Motion control of the flexible manipulator via controllable local degrees of freedom[J]. *Nonlinear Dynamics*, 2009, 55(4): 373–384.

[5] DI CASTRI C, MESSINA A. Exact modeling for control of flexible manipulators[J]. *Journal of Vibration and Control*, 2012, 18(10): 1526–1551.

[6] REDDY M P P, JACOB J. Accurate modeling and nonlinear finite element analysis of a flexible-link manipulator[J]. *International Journal of Mechanical, Aerospace, Industrial and Mechatronics Engineering*, 2014, 8(1): 165–170.

[7] DI CASTRI C, MESSINA A. Vibration analysis of a planar multilink manipulator using a reduced-order matrix formulation[J]. *Mechanics Research Communications*, 2011, 38(3): 231–238.

[8] ZHU Chunxia, LUO Jiman, WANG Dan, et al. Research on modal parameters identification of parallel manipulator with flexible multi-body system[J]. *Research Journal of Applied Sciences, Engineering and Technology*, 2013, 5(10): 2974–2979.

[9] XI F, FENTON R G. Exact modeling for control of flexible manipulators[J]. *The International Journal of Robotics Research*, 1994, 13(5): 443–453.

[10] GAO Zhihui, BIAN Yushu, YUN Chao. Coupling effect of flexible joint and flexible link on dynamic singularity of flexible manipulator [J]. *Chinese Journal of Mechanical Engineering*, 2008, 21(1): 9–12.

[11] VAKIL M, FOTOUHI R, NIKIFORUK P N, et al. A study of the free vibration of flexible-link flexible-joint manipulators[J]. *Proceedings of the Institution of Mechanical Engineers, Part C: Journal of Mechanical Engineering Science*, 2011, 225(6): 1361–1371.

[12] MEHREZ M W, EL-BADAWY A A. Effect of the joint inertia on selection of under-actuated control algorithm for flexible-link manipulators[J]. *Mechanism and Machine Theory*, 2010, 45(7): 967–980.

[13] AL-BEDOOR B O, ALMUSALLAM A A. Dynamics of flexible-link and flexible-joint manipulator carrying a payload with rotary inertia[J]. *Mechanism and Machine Theory*, 2000, 35(6): 785– 820.

[14] OGUAMANAM D C D, ARSHAD M. On the natural frequencies of a flexible manipulator with a tip payload[J]. *Proceedings of the Institution of Mechanical Engineers, Part C: Journal of Mechanical Engineering Science*, 2005, 219(11): 1199–1205.

[15] KALYONCU M, BOTSALI F M. Vibration analysis of an elastic robot Manipulator with prismatic Joint and A time-varying end mass [J]. *Arabian Journal for Science and Engineering*, 2004, 29(1): 27–38.

[16] TENG Youyou, CAI Guoping. Frequency characteristics of a flexible hub-beam system with arbitrary settling position of attached mass[J]. *Journal of Vibration and Control*, 2007, 13(6): 769–794.

[17] HUNG S C C, WENG C I. Modal analysis of controlled multilink systems with flexible links and joints[J]. *Journal of Guidance, Control, and Dynamics*, 1992, 15(3): 634–641.

[18] SETHI V, FRANCHEK M A, SONG G. Active multimodal vibration suppression of a flexible structure with piezoceramic sensor and actuator by using loop shaping[J]. *Journal of Vibration and Control*, 2011, 17(13): 1994–2006.

[19] RAJA S, SINHA P K, PRATHAP G. Active stiffening and active damping effects on closed loop vibration control of composite beams and plates[J]. *Journal of Reinforced Plastics and Composites*, 2003, 22(12): 1101–1121.

[20] MAXWELL N D, ASOKANTHAN S F. Modal characteristics of a flexible beam with multiple distributed actuators[J]. *Journal of Sound and Vibration*, 2004, 269(1): 19–31.

[21] KERMANI M R. Analytic modal analyses of a partially strengthened Timoshenko beam[J]. *IEEE Transactions on Control Systems Technology*, 2010, 18(4): 850–858.

[22] BENJEDDOU A. Advances in piezoelectric finite element modeling of adaptive structural elements: a survey[J]. *Computers & Structures*, 2000, 76(1): 347–363.

[23] BRATLAND M, HAUGEN B, ROLVAG T. Modal analysis of active flexible multibody systems[J]. *Computers & Structures*, 2011, 89(9): 750–761.

[24] CHEAH C C. Task-space PD control of robot manipulators: unified analysis and duality property[J]. *The International Journal of Robotics Research*, 2008, 27(10): 1152–1170.

[25] ISLAM S, LIU P X. PD output feedback control design for industrial robotic manipulators[J]. *IEEE-ASME Transactions on Mechatronics*, 2011, 16(1): 187–197.

[26] HECKMANN A. On the choice of boundary conditions for mode shapes in flexible multibody systems[J]. *Multibody System Dynamics*, 2010, 23(2): 141–163.

Biographical notes

CHU Ming, born in 1983, is currently an associate professor at *Automation School, Beijing University of Posts and Telecommunications, China*. He received his PhD degree from *Beijing University of Posts and Telecommunications, China*, in 2010. His research interests include flexible dynamics modeling, vibration control and intelligent robotics.
Tel: +86-10-61198259; E-mail: chuming_bupt@bupt.edu.cn

ZHANG Yanheng, born in 1978, is currently an associate professor at *Automation School, Beijing University of Posts and Telecommunications, China*. He received his PhD degree from *Beihang University, China*, in 2008. His research interests include robot structure design and pipeline robot.
Tel: +86-10-62281368; E-mail: zyh620@bupt.edu.cn

CHEN Gang, born in 1982, is currently an associate professor at *Automation School, Beijing University of Posts and Telecommunications, China*. He received his PhD degree from *Beijing University of Posts and Telecommunications, China*, in 2011. His research interests include robot motion planning.
Tel: +86-10-61198259; E-mail: chengang_zdh@bupt.edu.cn

SUN Hanxu, born in 1960, is currently a professor at *Automation School, Beijing University of Posts and Telecommunications, China*. He received his PhD degree from *Beihang Universtiy, China*, in 1989. His research interests include space robotics.
Tel: +86-10-62281011; E-mail: hxsun@bupt.edu.cn